For a point-by-point response to the reviews, please see the files submitted in December 2015

MARKED-UP MANUSCRIPT

blue: changes according to Reviewer #1

red: changes according to Reviewer Revel

green: other changes

A distal ~~145 ka~~ 140 ka sediment record of Nile discharge and East African monsoon variability

W. Ehrmann [1], **G. Schmiedl** [2], **M. Seidel** [1], **S. Krüger** [1], **and H. Schulz** [3]

[1] Universität Leipzig, Institut für Geophysik und Geologie, Talstraße 35, D-04103 Leipzig, Germany

[2] Universität Hamburg, Centrum für Erdsystemforschung und Nachhaltigkeit, Bundesstraße 55, D-20146 Hamburg, Germany

[3] Universität Tübingen, Fachbereich Geowissenschaften, Hölderlinstraße 12, D-72074 Tübingen, Germany

Correspondence to: W. Ehrmann (ehrmann@rz.uni-leipzig.de)

Abstract

Clay mineral assemblages in a sediment core from the distal Nile discharge plume off Israel have been used to reconstruct the late Quaternary Nile sediment discharge into the Eastern Mediterranean Sea (EMS). The record spans the last ca. 140 ka ~~145 ka~~. Smectite abundances indicate the influence of the Blue Nile and Atbara that have their headwaters in the volcanic rocks of the Ethiopian highlands. Kaolinite abundances indicate the influence of wadis, which contribute periodically to the suspension load of the Nile.

Due to the geographical position, the climate and the sedimentary framework of the EMS is controlled by two climate systems. The long-term climate regime was governed by the African monsoon that caused major humid periods with enhanced sediment discharge at 132 to <126 ka (AHP5), 116 to 99 ka (AHP4), and 89 to 77 ka (AHP3). ~~132 to <122 ka (AHP 5), 113 to 104 ka (AHP 4), and 86 to 74 ka (AHP 3).~~ They lasted much longer than the formation of the related sapropel layers S5 (>2 ka), S4 (3.5 ka) and S3 (5 ka). During the last glacial period (MIS 4–2) the long-term changes of the monsoonal system were superimposed by millennial-scale changes of an intensified mid-latitude glacial system. This climate regime caused short but pronounced drought periods in the Nile catchment, which are linked to Heinrich Events and alternate with more humid interstadials.

The clay mineral record further implies that feedback mechanisms between vegetation cover and sediment discharge of the Nile are detectable but of minor importance for the sedimentary record in the southeastern Mediterranean Sea during the investigated African Humid Periods.

1 Introduction

The Nile in northern Africa is the longest river of the world and the dominant sediment source for the Eastern Mediterranean Sea (Milliman and Syvitski, 1992). Its drainage basin is about 3 x 10^6 km^2 (Garzanti et al., 2015) and extends from the equator to ca. 30°N (Fig. 1). The main tributaries of the Nile are the perennial White Nile originating from Lake Victoria in tropical East Africa and the highly seasonal Blue

Nile and Atbara originating from the subtropical Ethiopian highlands. Downstream of the confluence, the Nile flows for more than 2000 km through the hyperarid Sahara. ~~On the way from the catchment to the delta, the Nile flows through different climate zones, from a cool and humid climate in the Ethiopian highlands to a hot and arid climate in Egypt.~~

Because of this special geographical situation, the runoff of the Nile is sensitive to climatic changes, and its discharge sediments are major recorders of the geological and climatic conditions in the catchment areas. The Nile sediments mainly reflect the intensity of rainfall in the headwaters, which has direct control on weathering, erosion and transport of sediments (Krom et al., 2002; Revel et al., 2010; Box et al., 2011; Garzanti et al., 2015). The present-day summer floods of the Nile are linked to a northward movement of the Intertropical Convergence Zone (ITCZ) and the African Rain Belt (ARB; Fig. 1) causing especially intense precipitation in July and August ~~especially~~ in the Ethiopian highlands.

Prior to the emplacement of the Assuan High Dam in 1964, the Nile carried a suspension load of about 120–160 x 10^6 t yr^{-1} to the Eastern Mediterranean Sea (EMS) (Holeman, 1968; Milliman and Syvitski, 1992; Stanley and Wingerath, 1996a). More than 95% of the material is derived from the Ethiopian highlands via Blue Nile and Atbara. In contrast, the sediment discharge ~~whereas the load~~ of the White Nile can be neglected because it´s load stored in Lake Victoria, Lake Albert and in the Sudd basin of South Sudan (Adamson et al., 1980; Foucault and Stanley, 1989; Williams et al., 2006; Williams et al., 2015; Garzanti et al., 2015). About 32.5% of the Nile suspension consists of clay (Quelennec and Kruc, 1976). Most of the silt- and sand-sized sediment accumulates in the Nile delta, on the Nile cone and along the Mediterranean shelf, whereas the clay-sized sediment fraction is transported in suspension by the surface currents of the Mediterranean Sea to the east and north (Fig. 1; Venkatarathnam and Ryan, 1971; Foucault and Mélières, 2000; Hamann et al., 2009).

It is well known that past changes in the amount of rainfall in the Ethiopian highlands were caused by precession-driven shifts in the position of the ITCZ that influenced the intensity and the spatial extent of the monsoon (e.g. Rossignol-Strick, 1983; Emeis et al., 2003). During African Humid Periods (AHPs) the spreading of the

vegetation cover in North Africa resulted in a “green” Sahara (Renssen et al., 2006; Kröpelin et al., 2008) and a reduced influx of Saharan dust into the Mediterranean Sea (deMenocal et al., 2000; Ehrmann et al., 2013). The increased runoff of the Nile River and of other North African river/wadi systems ~~Nile River runoff~~ brought huge amounts of freshwater and nutrients to the Mediterranean Sea, leading to enhanced productivity in the surface water, stagnation in the deep marine basin and formation of sapropel layers (Rossignol-Strick et al., 1982; Rohling, 1994; Emeis et al., 2003; Rohling et al., 2015). Although numerous studies concentrated on the Holocene AHP, very little is known about timing and intensity of former AHPs. Marine proxy data across sapropel S5 suggest that during the Eemian period (MIS 5e) the African monsoon was particularly strong and the African rain belt was shifted even further north than during the early Holocene. This resulted in flooding into the EMS through wadi systems along the wider North African margin (Rohling et al., 2002a; Osborne et al., 2008).

Different opinions exist on whether Nile sediment discharge is primarily controlled by precipitation and runoff, and thus closely linked to changes in the monsoon intensity (Wehausen and Brumsack, 2000; Emeis et al., 2000; Revel et al., 2010), or whether feedback mechanisms play an important role, with vegetation protecting soils and weathering products in the source area from being eroded (Adamson et al., 1980; Krom et al., 2002; Box et al., 2011).

A comprehensive effort to reconstruct Nile discharge during the last 100 ka was undertaken using the Fe content in sediments recovered from the proximal Nile delta (Revel et al., 2010; Caley et al., 2011). Most other geochemical investigations concentrated on shorter time spans and used different parameters such as K/Al, Mg/Al, Ti/Al, Ba/Ca to characterise the Nile discharge (Wehausen and Brumsack, 2000; Box et al., 2011; Weldeab et al., 2014). Several studies include the isotopic fingerprint of Nile sediments to reconstruct the Nile history (Krom et al., 1999a; Weldeab et al., 2002; Box et al., 2011; Blanchet et al., 2014).

We choose a different approach of reconstructing the Nile River sediment supply throughout the last some 140 ka ~~145 ka~~ by mainly investigating the content of typical Nile-derived clay minerals in sediment core GeoTü SL110, which was recovered from the distal Nile discharge plume off Israel (Fig. 1). Some 80% of the terrigenous

sediment fraction of the surface sediments near SL110 is derived from the Nile (Krom et al., 1999b), and is characterised by a high smectite content (e.g. Venkatarathnam and Ryan, 1971; Foucault and Mélières, 2000). By analysing a distal core from the plume, we document the Nile discharge activity as a whole rather than the activity of only a single channel in the delta.

2 Material

The investigated sediment core GeoTü SL110 was recovered from the SE Levantine Sea (Fig. 1, Table 1) during cruise M51/3 of the German research vessel "*Meteor*" in 2001 (Hemleben et al., 2003). It was retrieved at the Israeli continental slope off Haifa from a water depth of 1437 m. The sediments of the 652 cm long core mainly consist of muds with traces of pteropods and foraminifers. The core top contains basically undisturbed surface sediments as indicated by the presence of an oxidised layer. The muds show frequent diffuse colour changes, mainly between grey and olive grey. Darker sapropel layers (greenish black, dark greenish grey, dark grey) occur at 35–61 cm (S1, with a possible interruption at 44–45 cm), 500–514 cm (S3), 558–570 cm (S4) and 598–622 cm (S5, including pre-sapropelic layer). The core does not show any indications for slumping, debris flows or turbidites but indicates rather constant sedimentary conditions in the distal discharge plume of the Nile. No tephra layers were detected.

3 Methods

The lightness (L^*) of core SL110 was determined in 1 cm steps with a Minolta colour spectrophotometer immediately after opening of the core.

The content of total organic carbon (TOC) was measured on 174 ground bulk sediment samples with an Eltra METALYST-CS-1000-S after removal of carbonate with HCl.

The core was sampled in 1 cm intervals for investigations of the grain size composition of the terrigenous sediment fraction and of the clay mineral

assemblages. The samples were oxidized and disaggregated by means of 5% hydrogen peroxide. Carbonate was dissolved by 10% acetic acid. We isolated the terrigenous sand fraction by sieving the samples through a 63 µm mesh. The silt fraction (2–63 µm) was separated from the clay fraction (<2 µm) in settling tubes.

The analyses of the clay mineral composition followed standard methods (e.g. Ehrmann et al., 2007). We added MoS_2 as an internal standard to the clay suspension. Texturally oriented clay mounts were solvated with ethylene–glycol vapour at a temperature of 60°C and then X-rayed with a Rigaku MiniFlex system (CoKα radiation; 30 kV; 15 mA). We analysed the samples in the range 3–40° 2Θ with a step size of 0.02° 2Θ and a measuring time of 2 s step^{-1}. In addition, we analysed the range 27.5–30.6° 2Θ with a step size of 0.01° 2Θ and a measuring time of 4 s step^{-1} in order to better resolve the (002) peak of kaolinite and the (004) peak of chlorite. We evaluated the diffractograms by using the MacDiff software (Petschick, 2001). After adjusting the diffractograms to the MoS_2 peak at 6.15 Å, we deconvoluted the peak doublets smectite/chlorite (17/14 Å), palygorskite/illite (10.5/10 Å) and kaolinite/chlorite (3.58/3.54 Å). We based the semi-quantitative estimations of the clay mineral abundances on the integrated peak areas of the individual peaks and weighting factors (Biscaye, 1964; 1965; Weaver and Beck, 1977). ~~For palygorskite, we used the same factor as for chlorite and kaolinite.~~

4 Age Model

For establishing a stable oxygen isotope stratigraphy we analysed tests from the 250–355 µm size fraction of the surface-dwelling foraminifer species *Globigerinoides ruber* (white) of about 130 samples using a Kiel IV online carbonate preparation line connected to a MAT 253 mass spectrometer. The values are reported in ‰ relative to VPDB using the delta notation. The reproducibility was better than ±0.06‰ (1σ). Age points were derived by a graphic correlation of our $\delta^{18}O$ record with the *G. ruber* (white) $\delta^{18}O$ data of sediment core LC21 from the southern Aegean Sea (Grant et al., 2012), ~~a standard stack (Lisiecki and Raymo, 2005)~~ aided by the software AnalySeries 2.0 (Paillard et al., 1996) (Table 2, Fig. 2). The LC21 chronology was constructed by using ^{14}C dating and by tuning its $\delta^{18}O$ record to the U/Th-dated Soreq Cave speleothem $\delta^{18}O$ record (Grant et al., 2012).

Further age control comes from four ^{14}C-accelerator mass spectrometry (AMS) datings performed by Beta Analytic Radiocarbon Dating Laboratory on well-preserved shells of planktonic foraminifera (*G. ruber, G. bulloides, G. sacculifer, O, universa*) that represent the age of the surface waters. We applied an eastern Levantine Sea Delta-R of 3 ± 66 years (Marine Reservoir Database). The radiocarbon ages were converted to calendar years using the Marine13 data base (Reimer et al., 2013; Table 2).

We identified a hiatus at 598 cm, at the top of the S5 interval, based on several arguments. The lower part of the dark interval between 622 and 604 cm is characterised by only about 0.8% TOC (Fig. 3a), by the occurrence of a relatively diverse benthic foraminiferal assemblage containing *G. orbicularis*, *G. translucens* and *C. laevigata*, and by relatively high δ^{18}O values (Fig. 3a). Despite the dark colour, this indicates a pre-sapropelic interval at the transition between Marine Isotope Stages (MIS) 6 and 5 rather than a full sapropel (Schmiedl et al., 2003). The TOC concentrations start to rise to ca. 1.4% at 603 cm. We therefore assume the base of sapropel S5 at 603 cm, with an age of 128.0 ka (Grant et al., 2012). ~~124.0 ka (Bar-Matthews et al., 2000; Rohling et al., 2002b; Morigi, 2009; Osborne et al., 2010).~~ The TOC values drop abruptly to 0.5% at 596 cm. Thus, the TOC concentrations remain below the typical values of 2–3% in S1, S3, S4 (Fig. 3a) and in S5 of nearby core KL83 (Weldeab et al., 2003). Also the analysis of the benthic foraminifera showed an extremely thin anoxic phase in SL110, compared to a 27 cm thick S5 in KL83 (Schmiedl et al., 2003). Thus, most of S5 is missing in SL110 due to a hiatus that was probably caused by a slump as indicated by the sharp and curved lithological boundary at 598 cm. By comparing our δ^{18}O record with standard curves and the record of MD84-641 (Table 1, Kallel et al., 2000) and considering an age of 128–121 ka for S5 (Grant et al., 2012) we argue for an extrapolated age of the hiatus from 126–119 ka. ~~the published age of 124 to 119 ka for S5 (Bar-Matthews et al., 2000; Rohling et al., 2002b; Morigi, 2009; Osborne et al., 2010) we argue for an extrapolated age of the hiatus from 122 ka to 115 ka.~~ In nearby core GeoTü KL83 (Table 1), Weldeab et al. (2002, 2003) identified a hiatus spanning the period 110–70 ka, with the base of the hiatus at 13 cm above S5.

For consistency reasons, we also adapted the age model of core GeoTü SL143 (Ehrmann et al., 2013; Fig. 4) by using basal ages of 86.0 ka and 108.0 ka for sapropels S3 and S4, respectively, according to the LC21 record (Grant et al., 2012)

5 Results

The raw data of our investigations on sediment core GeoTü SL110 ~~are stored in the PANGAEA data base at the Alfred Wegener Institute for Polar and Marine Research, Bremerhaven, Germany (http://doi.pangaea.de/10.1594/PANGAEA.848291) and~~ are presented in Fig. 3, which also shows the positions of the sapropel layers S1, S3, S4 and S5.

The $\delta^{18}O$ data of *G. ruber* go back to MIS 6 (Fig. 3a ~~Figs. 2, 3a~~). The Last Glacial Maximum has values of ca. 3‰, whereas the minimum values during interglacials MIS 1 and MIS 5 are around –1.5‰.

The lightness data (*L**, Fig. 3a) reflect subtle colour changes within the core. The darkest intervals correlate with the sapropels (*L** ca. 37). However, also large parts of the other muds are relatively dark (*L** ca. 40–45). The lightest interval occurs ~~at 625–640 cm, corresponding to~~ during the MIS 6 interval 132–135 ka.

TOC contents generally fluctuate between 0.4 and 0.7%, but increase to 2.5–3% in the sapropel layers S1, S3 and S4, and to 1.5% in the pre-sapropelic layer of S5.

The terrigenous sand content is generally <4%, the silt/clay ratio <1.0. The data sets show the same general pattern (Fig. 3a) with finer grained intervals ~~around 0–60, 490–515, 550–570, 600–620 cm and enclose~~ enclosing the sapropel layers. A distinct coarse interval occurs at 132–135 ka ~~625–640 cm~~. Between 73 and 18 ka ~~480 and 110 cm~~ we observe an upward coarsening trend. The high silt/clay ratio at ca. 17 ka ~~(103–102 cm)~~ reflects a thin, light gray, not graded silt layer consisting almost entirely of quartz grains.

The clay mineral assemblage of SL110 (Fig. 3b) is dominated by smectite that fluctuates between ca. 30% ~~35%~~ and 65%. Maximum values occur around 3, 31–37,

46, 50–59, 65–69, 77–89, 99–116, and 127–132 ka ~~(15, 210–260, 315, 340–400, 460, 490–525, 545–585 and 600–625 cm)~~. Minimum values occur at 132–135 ka ~~625–640 cm~~. Illite shows an opposite distribution pattern with concentrations ranging between 5 and 25%. Kaolinite concentration fluctuates between 20% and 30% and shows only a few distinct maxima centred at 95, 116 and 133 ka, ~~540 cm, 590 cm and 630 cm,~~ and minima at 0–5, 35, 87, 111 and 128–132 ka ~~0–30, 230–250, 520, 570 and 600–620 cm~~. Chlorite is present in low concentrations of 7–11%, with a pattern roughly resembling that of kaolinite. Palygorskite occurs in trace amounts throughout the core, but jumps to 4% at 132–135 ka ~~625–640 cm~~.

6 Discussion

Sedimentation at SL110

According to our age model (Fig. 2, Table 2), sediment core SL110 has an extrapolated basal age of ca. 137 ka ~~145 ka~~. The linear sedimentation rates are 2.2 to 9.8 ~~8.8~~ cm/ka (Fig. 3a). They are low during ~~late MIS 6 and~~ MIS 5, and distinctly higher in late MIS 6 and MIS 4 ~~MIS 3~~ to MIS 1. Sedimentation rates for nearby core MD84-641, extracted ~~calculated~~ from data by Fontugne and Calvert (1992), show less distinct changes ~~a similar pattern~~ (Fig. 2) and ~~but~~ are distinctly lower than in SL110 due to its further offshore position.

The non-carbonate sediment fraction of seafloor surface sediments in the region of SL110 is dominantly derived by long-distance sediment transport from the Nile (Venkatarathnam and Ryan, 1971; Stanley et al., 1997; 1998; Krom et al., 1999b; Weldeab et al., 2002; Hamann et al., 2009). Storm waves and coastal currents erode coarse sediments from the delta. Geostrophic and wave-induced near-shore and shelf currents displace this material in a large counter-clockwise current along the coast towards the Levantine Sea (Fig. 1) and deposit it in the shallow waters off Israel. The fine fraction, in contrast, is derived from direct input from the Nile into the sea and may be transported also further offshore and further to the north (e.g. Stanley et al., 1997; 1998; Venkatarathnam and Ryan, 1971; Foucault and Mélières, 2000). Aeolian influx from the Sahara and riverine supply of small Near East rivers and wadis are only of minor importance (Stanley et al., 1997; Sandler and Herut,

2000). The enhanced glacial sedimentation rates observed in core SL110 might be a result of stronger currents and/or a shift of the currents and therewith of the high-accumulation areas to a more seaward position due to a lower sea level. These processes may also be responsible for the coarsening of the sediments as indicated by the terrigenous sand content and the silt/clay ratios (Fig. 3a).

The increasing glacial sedimentation rates theoretically also could be explained by increasing aridity resulting in an enhanced influx of aeolian dust. Endmember modelling of the terrigenous silt fraction of the nearby core SL112 (892 m water depth), which is located closer to the coast, indicates increased dust fluxes during the LGM and the late glacial (Hamann et al., 2008). However, such an influx is not documented in the clay mineral record of SL110, e.g. by the concentration of wind-blown palygorskite (Fig. 3b). In addition, glacial sedimentation rates at site SL112 were lower when compared to the Holocene, thus supporting the interpretation of a glacial-interglacial shift of the high-accumulation zone.

Clay Mineral Assemblages

Smectite in southeastern Levantine Sea sediments is generally regarded to be of detrital origin and is the typical clay mineral in Nile-derived sediments (Venkatarathnam and Ryan, 1971; Maldonado and Stanley, 1981; Stanley and Wingerath, 1996a; Foucault and Mélières, 2000). According to the compilation by Hamann et al. (2009), the Nile assemblage contains up to 85% smectite. Kaolinite is the second important clay mineral with concentrations in the order of 20%. Illite contents are <10%, and chlorite occurs in trace amounts. ~~The Nile incorporates almost its entire suspension load close to its source (Adamson et al., 1980).~~

The riverine suspension load is reflected in the modern clay mineral assemblage in seafloor surface sediments of the SE Levantine Sea. Accordingly, the clay mineral assemblage off southern Israel consists of up to >70% smectite, 10–25% kaolinite, 10% illite and <10% chlorite (Hamann et al., 2009) and thus reflects the Nile source. The uppermost samples of core SL110 with ca. 60% smectite, 22% kaolinite, 8% illite and 9% chlorite fit well into this distribution pattern.

The composition of the aeolian clay mineral assemblage reaching the SE Levantine

Sea is variable, but generally characterized by high illite and kaolinite concentrations (Chester et al., 1977). Palygorskite is a typical clay mineral in aeolian dust derived from the Sahara (Foucault and Mélières, 2000; Scheuvens et al., 2013).

The Nile incorporates almost its entire suspension load close to its source (Adamson et al., 1980). The smectite comes with the Nile suspension load from the catchment of the Blue Nile and Atbara rivers and originates from weathering of Cenozoic volcanic rocks on the Ethiopian Plateau (e.g., Stanley and Wingerath, 1996a). The White Nile south of the confluence of Sobat river, also discharging the Ethiopian highlands, shows a considerably different clay mineral signature with significantly lower smectite contents. Alluvial sediments from central Uganda have smectite contents <20% (Nyakairu and Koeberl, 2001); no smectite was described from lake-bottom sediments of Lake Victoria (Mothersill, 1976). Tropical weathering in the equatorial region produces only small amounts of smectite (Garzanti et al., 2015). Furthermore, the smectite content in SL110 correlates with the Fe content documented by Revel et al. (2010) in delta sediments of the Nile, especially during humid periods. Because Fe is unequivocally derived from the volcanic rocks of the Ethiopian highlands, this also suggests that the overwhelming part of the smectite comes from that source.

Sediments of the Egyptian wadis discharging into the Nile have clay mineral assemblages with typically 40–55% kaolinite, 35–45% smectite and 5–15% illite (Stanley and Wingerath, 1996b; Hamann et al., 2009; chlorite not determined, thus, actual kaolinite concentrations may be somewhat lower). The kaolinite is mainly derived from the erosion of kaolinite-rich Eocene, Palaeocene and Mesozoic sediments and lateritic soils in the wadis (Stanley and Wingerath, 1996b; Bolle et al., 2000). Theoretically, the White Nile could also deliver kaolinite during certain times of enhanced sediment transport during humid periods (Garzanti et al. 2015). This would result in a decrease in smectite at the same time due to dilution. This, however, is not the case (Fig. 3b). Therefore we argue that the kaolinite accumulating in SL110 predominantly comes from the North African wadi regions.

~~The composition of the aeolian clay mineral assemblage reaching the SE Levantine Sea is variable, but generally characterized by high illite and kaolinite concentrations (Chester et al., 1977). Palygorskite is a typical clay mineral in aeolian dust derived~~

~~from the Sahara (Foucault and Mélières, 2000; Scheuvens et al., 2013).~~

~~The clay mineral assemblage in the seafloor surface sediments of the SE Levantine Sea off southern Israel consists of up to >70% smectite, 10–25% kaolinite, 10% illite and <10% chlorite (Hamann et al., 2009) and thus reflects the Nile source. The uppermost samples of core SL110 with ca. 60% smectite, 22% kaolinite, 8% illite and 9% chlorite fit well into this distribution pattern.~~

According to the standard method, percentages of the clay minerals smectite, illite, chlorite, kaolinite and palygorskite add up to 100%. A change in the abundance of one mineral therefore causes also changes in the concentration of the others. Hence we prefer to discuss clay mineral ratios. We use Sm_r = smectite/(illite+chlorite) as the main proxy for Nile discharge provided by the Blue Nile and Atbara, and Ka_r = kaolinite/(illite+chlorite) as an indicator for the contribution of the wadis.

The good correlation between the Ka_r and the Sm_r data (Fig. 4; r^2 = 0.73) confirms that the kaolinite in SL110 is of fluvial origin (Venkatarathnam and Ryan, 1971; Stanley and Wingerath, 1996a; Hamann et al., 2009), and not derived by aeolian influx from the Sahara, as in other regions of the EMS (e.g. Chester et al., 1977; Foucault and Mélières, 2000; Ehrmann et al., 2013). The correlation implies that during times of enhanced Nile runoff and smectite transport from Ethiopia, the erosion of kaolinite-rich sediments and soils in the wadis was generally also active, and that during dry periods in Ethiopia the wadis were dry, too.

This confirms earlier findings based on the interpretation of satellite images and sedimentological investigations, which showed that extensive drainage systems were active in the eastern Sahara during humid phases, especially of Eemian and Holocene time (e.g. Pachur and Hoelzmann, 2000; Rohling et al., 2002b; Osborne et al., 2008). Furthermore, oxygen isotope data from speleothems of Soreq Cave (Bar-Matthews et al., 2000) imply that rainfall extended beyond the Sahara.

The clay mineral data of SL110 document a highly variable smectite and kaolinite input through time (Figs. 3b, 4) and show similar distribution patterns as the Fe record from the Nile delta (Revel et al., 2010; Caley et al., 2011). Fe is supposed to be derived from weathering of volcanic rocks in the Atbara and Blue Nile headwaters

in the Ethiopian highlands, and thus changing Fe contents may reflect changing precipitation regimes. Furthermore, the smectite and kaolinite distribution patterns are inversely correlated to the record of Saharan dust in the central Aegean Sea core GeoTü SL143 (Ehrmann et al., 2013).

Penultimate Glacial Period

The oldest part of the record displays minimum Sm_r and Ka_r values at ca. 135-132 ka of MIS 6 (Fig. 4). The lack of sediment derived from the Nile delta indicates that the site was not within the range of the Nile deep-sea turbidite system postulated for MIS 6 at ca. 33°30´to 33°50´E (Ducassou et al. 2009). The clay mineral data point ~~pointing~~ to extremely dry conditions for the penultimate glacial maximum ~~at ca. 142-132 ka of MIS 6 (core interval 646-624 cm, age uncertainties >135 ka because of extrapolation)~~. The extreme drought possibly correlates with Heinrich Event 11, which is known as a very cold period in the Western Mediterranean Sea and dated to 135-130 ka (Martrat et al., 2014; Marino et al., 2015). Obviously, only minor amounts of Nile suspension load reached the coring site off Israel. Instead, maximum palygorskite concentrations (Fig. 3b) and high proportions of terrigenous silt and sand (Fig. 3a) document an increased aeolian influx from the Sahara. This arid phase seems to have been more severe than that of the Last Glacial Maximum. After the maximum drought of MIS 6 the record of SL110 show a sharp transition to a sapropelic event embedded in an AHP.

Sapropel Formation

It is well known that sapropel formation was coupled to precession-related maxima in northern hemisphere summer insolation causing a northward shift of the ITCZ, an intensification of the African monsoon system and enhanced precipitation in the Ethiopian highlands (e.g. Rossignol-Strick, 1983; Rohling, 1994; Emeis et al., 2003; Rohling et al., 2015). In SL110, high Sm_r, Ka_r and low silt/clay ratios occur mainly during interglacial periods with negative $\delta^{18}O$ values and indicate phases with enhanced Nile and wadi discharge of fine-grained suspension to the Levantine Sea accompanying formation of sapropels S5, S4, S3 and S1. The enhanced rainfall under a warm climate caused stronger chemical weathering of the volcanic rocks and thus smectite formation. The enhanced river runoff contributed to the stratification of

the water column and facilitated the transport of nutrients and weathering products to the EMS promoting ~~enhanced surface water productivity at least~~ a shoaling of the nutricline and thus development of a deep chlorophyll maximum (Rohling and Gieskes, 1989; Grelaud et al., 2012) particularly in areas close to the Nile delta. These processes fostered sustained anoxic conditions in the deeper basins and preservation of TOC (Fig. 3a).

Both the clay mineral record of southeastern Levantine Sea core SL110, the Fe record from the Nile delta (Revel et al., 2010; Caley et al., 2011) and the record of Saharan dust influx to the Aegean Sea (Ehrmann et al., 2013) reveal that each phase of sapropel formation occurred within a longer AHP (Fig. 4; AHPs numbered according to the corresponding sapropels).

The last Interglacial Period

The Sm_r maximum linked to AHP 5 shows a sharp onset after the glacial maximum of MIS 6, simultaneously with the start of the pre-sapropelic layer of S5 (Fig. 4). It indicates a northward moving rain belt resulting in enhanced monsoonal rainfall in Ethiopia and Blue Nile runoff as early as 132 ka at a time of increasing insolation but under the influence of penultimate glacial boundary conditions. Also the Ka_r values clearly increase with the beginning of the pre-sapropelic layer. However, they do not exhibit such distinct maximum values as during the early phases of the younger AHPs. Most of sapropel S5 and the termination of AHP 5, however, are not preserved in SL110 due to the hiatus at ca. 126–119 ka ~~122–115 ka~~. Furthermore, because of the curved top of the sapropel and the technique of sampling the core in parallel slices, we did not receive the typical sapropel signature but a mixed sapropel/post-sapropel signal (Fig. 4).

According to the Fe and the dust record (Revel et al., 2010; Ehrmann et al., 2013), AHP 4 started at >108 ka and lasted until 95 ka or 98 ka, respectively. The Sm_r and Ka_r data of SL110 indicate that AHP 4 started during insolation rise at 116 ka and ended at 99 ka, with sapropel formation occurring at 108–104.5 ka (Fig. 4).

~~According to the Fe and the dust record, AHP 4 lasted from >105 ka to ca. 95 ka (Revel et al., 2010; Ehrmann et al., 2013). The Sm_r and Ka_r data of SL110 indicate~~

~~that AHP 4 started during insolation rise at 113 ka and ended at 94 ka, with sapropel formation occurring at 105–99.5 ka (Fig. 4).~~

AHP 3 started just before the insolation maximum and lasted ca. 89–77 ka ~~86–74 ka~~ based on the Sm_r and Ka_r maxima and the minima in the silt/clay ratio and the terrigenous sand content. These ages are in good accordance with those obtained from the dust record in the Aegean Sea (Ehrmann et al., 2013). Sapropel S3 has a shorter duration and spans the time interval 86–81 ka ~~82–77.5 ka~~.

Despite the hiatus in the SL110 record, by assuming a duration of 128–121 ka for S5 (Grant et al., 2012) ~~124–119 ka for S5 (Bar-Matthews et al., 2000; Rohling et al., 2002b; Morigi, 2009; Osborne et al., 2010)~~, our data indicate that the dry phase between AHP 5 and AHP 4 lasted only ca. 5 ka, compared with ca. 11 ka for the one between AHP 4 and AHP 3 ~~ca. 6 ka, and the one between AHP 4 and AHP 3 only ca. 8 ka~~. It is interesting to note that a similar duration of the dry phases can be deduced from the pollen record of Tenaghi Philippon in Greece, although this remote site is governed dominantly by northern climatic factors (Tzedakis, 2005; Pross et al., 2015).

The last Glacial Period

After a further short dry period at 77–70 ka ~~74–68 ka~~, Sm_r, Ka_r and silt/clay ratios indicate humid phase AHP 2 and enhanced Nile runoff in early MIS 4 at 69–65 ka ~~68–64 ka~~. It is of similar magnitude as the interglacial AHPs discussed before and also starts during increasing insolation (Fig. 4). In contrast to the previous AHPs this one is not accompanied by low $\delta^{18}O$ values. It is also not accompanied by a sapropel, dark sediment colour or enhanced TOC values (Fig. 3a). However, it coincides with the common occurrence of shallow infaunal *Uvigerina peregrina*. This highly opportunistic species is adapted to the seasonal deposition of high amounts of fresh phytodetritus (Koho et al., 2008). In analogy to nearby SL112, the occurrence of this species at site SL110 during AHP 2 is likely fuelled by pronounced algal blooms related to seasonally enhanced Nile runoff and nutrient supply (Schmiedl et al., 2010). However, in core SL110 we have strong indications that AHP 2 did not culminate in a sapropel formation. Sediment and nutrient delivery by the Nile was cut-off by a drought linked to Heinrich Event 6 occurring just at the time of maximum

insolation (Fig. 4). This drought, possibly combined with stronger winds and better ventilation of the deep waters, reduced sediment discharge into the Mediterranean Sea and hampered stagnation of the deep water and sapropel formation.

Lourens et al. (1996 ~~1966~~) described a thin sapropel layer S2, corresponding to AHP 2, south of Crete that occurs after the 60 ka insolation maximum. It was argued that this sapropel is not visible any more in most sedimentary sequences of the eastern Mediterranean Sea because of post-depositional oxidation of the organic matter (Emeis et al., 2000; Löwemark et al., 2006).

It is not understood why our clay mineral signal has no counterpart in the Fe signal from the Nile delta (Revel et al., 2010). Possibly Nile discharge to the Eastern Mediterranean Sea at that time was not via the western Rosetta branch, but via the eastern Damietta branch, and thus site MS27PT starved of sediment. It also cannot be ruled out that a match is obscured because of different age models, insofar as the Fe 73 ka peak corresponds to our well-dated 67 ka ~~68 ka~~ clay mineral peak (Fig. 4).

The slightly enhanced Sm_r and Ka_r values at 59–50 ka ~~58–48 ka~~ possibly document the late phase of AHP 2 after the termination of Heinrich Event 6, reflecting the re-occurrence of slightly enhanced Nile River runoff. Other indications for somewhat increased temperature, humidity and Nile influx during this time interval come from the Fe record in the Nile delta (Revel et al., 2010) and the $\delta^{18}O$ records of Soreq Cave and of sediment cores 9509 and 9501 in the eastern Levantine Sea (Almogi-Labin et al., 2009). The latter records show a marked drop in planktonic foraminiferal $\delta^{18}O$ values between 58 and 49 ka BP. The signal of warm and freshened surface waters was particularly expressed in core 9501 from the northern part of the basin and coincided with D-O interstadial 14. The spread of deciduous and other trees during the same time period likely supported the migration of anatomically modern humans from Africa into the Levant (Müller et al., 2011). In the Sm_r data of core SL110, this time interval documents only a moderate increase of Nile runoff (Fig. 4) suggesting that the observed warming and freshening of the eastern Mediterranean region was predominantly related to a high-latitude climate change.

Thus, the sediments of SL110 document that the long-term climate regime governed by the African monsoon and characterized by pronounced AHPs during the last

interglacial period was replaced as of the occurrence of Heinrich Event 6 by a distinctly different glacial climate system governed by short-term, millennial-scale climate changes having their origin in the North Atlantic and Arctic regions. Former studies showed that sudden freshwater influxes into the northern Atlantic Ocean during the Younger Dryas and the Heinrich Events not only weakened the thermohaline circulation and oceanic heat transport to the northern high latitudes (e.g. Bond et al., 1993), but also had major consequences for the Mediterranean Sea environment. Increased aridity and even North African mega-droughts during such events can be seen in marine sediments of the North Atlantic Ocean (Mulitza et al., 2008), speleothem data and lake level drops of Lake Lisan (palaeo-Dead Sea; Bar-Matthews et al., 1999; Bartov et al., 2003) and of African lakes (Gasse et al., 2008; Shanahan et al., 2015). Cold water influx from the North Atlantic Ocean to the Mediterranean Sea intensified. Sea surface temperatures and deep-water temperatures decreased and deep-water ventilation fortified in the northwestern Mediterranean Sea (Cacho et al., 1999; 2000) and probably also in the EMS. Enhanced northward flux of wind-transported sediment from the Sahara is documented for both the Western and the Eastern Mediterranean Sea (Moreno et al., 2002; Bout-Roumazeilles et al., 2007; Hamann et al., 2008). Strongly decreased Sm_r and Ka_r values in core SL110 (Fig. 4) indicate reduced Nile sediment discharge during Heinrich Events, and therewith major droughts in the headwaters of the Atbara and Blue Nile and diminished erosion and river runoff. During these events the ITCZ and the African Rain Belt moved southward. Both Lake Tana, the source of the Blue Nile, and Lake Victoria, the source of the White Nile, desiccated during the Younger Dryas and the Heinrich Event 1 (Lamb et al., 2007; Marshall et al., 2011). Minimum Sm_r and Ka_r values as well as the occurrence of a silt layer of probably aeolian origin (Fig. 3a) imply that Heinrich Event 1 was the driest interval since the MIS 6 glacial maximum (cf. Stager et al., 2011).

The 65°N insolation curve shows a further low-amplitude maximum at ca. 37 ka. It is also reflected by slightly enhanced smectite and kaolinite abundances in core SL110, ranging 37–31 ka ~~38–30 ka~~ and by the Fe record in the Nile delta (Revel et al., 2010). No sapropel formation was recorded following the weak insolation maximum at 37 ka. Thus, the two potential humid periods linked to the glacial insolation maxima at 60 and 37 ka are only vaguely expressed in the EMS, because their

effects were much less distinct and because they were suppressed by the glacial climate regime, particularly the impacts of cold and dry stadials.

The last African Humid Period and the Holocene

The clay mineral data of SL110 and of nearby core SL112 (Hamann et al., 2009) document a gradual onset of AHP 1 at about 14 ka ~~15 ka~~ (Fig. 4), which coincides with the overflow of Lake Tana, the source of the Blue Nile (Lamb et al., 2007; Marshall et al., 2011). At the same time, Saharan dust influx to the EMS decreased (Ehrmann et al., 2013). S1 at ca. 11–6.5 ka and the peak Blue Nile runoff at 10–9 ka (Weldeab et al., 2014) are only poorly reflected in the clay mineral data. Precipitation generally declined gradually after sapropel formation throughout the Holocene, the Nile River runoff responded quasi-linearly to the changes in rainfall (Weldeab et al., 2014; Blanchet et al., 2014), and the AHP 1 ended at ca. 5 ka (deMenocal et al., 2000). However, the clay mineral data do not mirror this trend but show continued increasing Sm_r and Ka_r values and Nile sediment discharge until ca. 2 ka. Sediment discharge thus is decoupled from water runoff. Possibly, human activity altered the natural signal. Saharan population increased shortly after 11 ka and reached a maximum at 7.5 ka (Manning and Timpson, 2014). Major land-use changes occurred with the advent of Neolithic farming some 8 ka ago (Williams, 2009).

Feedback Effects

The clay mineral and grain size data of SL110 indicate an enhanced riverine influx of suspension from the Blue Nile and Atbara to the Mediterranean Sea during the AHPs and therefore document enhanced weathering of the Ethiopian basalts, erosion of soils and transport of the suspension load to the sea. This view is supported by several investigations (Wehausen and Brumsack, 1998; Emeis et al., 2000; Revel et al., 2010; Blanchet et al., 2014). However, it is in conflict with some other studies (Adamson et al., 1980; Krom et al., 1999a; 2002; Box et al., 2011) that argued for a lower Blue Nile sediment discharge during the warm and humid Holocene AHP and higher fluxes during dry climate phases. They reasoned that at present the limited vegetation cover on the Ethiopian highlands allows extensive erosion when the summer monsoon rains fall. During increased monsoon activity, in contrast, longer

periods of rain, longer growing seasons and larger vegetation-covered areas reduced soil erosion.

Our data indicate that an increase in precipitation and Nile suspension delivery happened long before sapropel formation, during phases of increasing insolation. However, in the case of AHP 4 Sm_r and Ka_r maxima occur just before and after sapropel S4 formation, each accompanied by low silt/clay ratios also indicating enhanced riverine suspension (Fig. 3a). Thus, maximum riverine sediment influx does not coincide with maximum water discharge during sapropel formation. This is possibly due to a feedback mechanism as postulated, for example, by Adamson et al. (1980) and Krom et al. (2002). ~~Vegetation feedbacks were obviously not active in glacial time.~~ Vegetation feedbacks were obviously less expressed during glacial conditions, particularly during the last glacial maximum. This is linked to the generally more arid boundary conditions during the last glacial in tropical and northern Africa (Gasse, 2000) and resulting sparse vegetation cover, particularly in the deflation areas of the Sahara (Tjallingii et al., 2008). The rapid climate changes linked to Dansgaard-Oeschger cycles and Heinrich Events find immediate response in the sediment delivery to the EMS.

The different timing between the Saharan dust record and the Nile discharge record of the humid phases (Fig. 4) may reflect regional differences in the climatic history. The northward migrating tropical rain belt may first have reached the Ethiopian highlands, where the smectite signals has its origin, and with a time lag the central Sahara, there inhibiting effective dust production. The differences may also be due to different processes being at work. The Nile discharge is mainly driven by annual floods, fluvial erosion and weathering. It therefore may have reacted immediately on a northward shift of the ITCZ and the rain belt. The dust record, in contrast, is mainly a function of aridity, wind strength and, probably most important, the availability of deflatable material. The spreading and retreat of a vegetation cover plays an important role and may react non-linearly and with a different time lag on a shift of the ITCZ than river discharge (Claussen et al., 2013; Ehrmann et al., 2013). Thus, recently Blanchet et al. (2014) could show for the end of AHP 1 that the vegetation retreat from the Sahara was much faster than the decrease in Nile runoff during the southward migration of the rain belt.

7 Conclusions

– Clay minerals are suitable tools to reconstruct the late Quaternary Nile sediment discharge to the EMS. The abundance of smectite reflects the runoff of the Blue Nile and Atbara, whereas kaolinite abundance reflects the discharge from wadis. The correlation of smectite and kaolinite abundances implies that during times of enhanced Nile suspension discharge the wadis also were active sediment sources.

– High smectite and kaolinite abundances and low terrigenous silt/clay ratios indicate phases of enhanced precipitation and suspension influx from the Blue Nile, Atbara and the wadis to the Levantine Sea, the so-called African Humid Periods (AHPs), which are accompanied by the formation of sapropel layers. This largely contradicts the view that sediment delivery during humid periods was reduced because an extensive vegetation cover hampered soil erosion.

– Precipitation and suspension discharge started much earlier and ended later than sapropel formation. Maximum sediment discharge does not coincide with maximum water discharge during times of sapropel formation because of minor vegetation feedback.

– The time lag between the increase/decrease of Nile suspension discharge and the decrease/increase in the dust record (SL143) can be explained by a successive migration of the rain belt, possibly combined with a vegetation feedback.

– The dry periods between the interglacial AHPs were relatively short, each lasting only ca. 5–10 ka ~~ca. 6-8 ka~~.

– The sedimentary record of core SL110 demonstrates the interplay of two competing climate systems. The long-term climate regime was governed by the African monsoon and characterized by pronounced AHPs during the last interglacial period. This system was replaced in the last glacial by short-term, millennial-scale climate changes having their origin in the North Atlantic region. They are characterised by short but pronounced drought periods linked to Heinrich Events and more humid interstadials. Precipitation in the Nile catchment, river runoff and

sapropel formation can be hampered or even inhibited under the influence of the North Atlantic climate system, particularly under glacial boundary conditions.

Data Availability: The raw data to this article ~~is available at http://dx.doi.org/10.1594/PANGAEA.848291.~~ are stored in the PANGAEA data base at the Alfred Wegener Institute for Polar and Marine Research, Bremerhaven, Germany (http://doi.pangaea.de/10.1594/PANGAEA.848291).

Acknowledgements. We thank the chief scientist C. Hemleben, the master and the crew of “RV Meteor” for their support during cruise 51/3. For technical assistance in the laboratory we thank S. Haeßner and M. Haeßner. C. Kertscher performed some TOC analyses. M. Paul is acknowledged for picking foraminifera and establishing a preliminary age model. We acknowledge M. Revel and an anonymous reviewer for their comments that helped improving our manuscript. The Deutsche Forschungsgemeinschaft (DFG) financially supported this study.

References

Adamson, D. A., Gasse, F., Street, F. A., and Williams, M. A. J.: Late Quaternary history of the Nile, Nature, 288, 50–55, 1980.

Almogi-Labin, A., Bar-Matthews, M., Shriki, D., Kolosovsky, E., Paterne, M., Schilman, B., Ayalon, A., Aizenshtat, Z., and Matthews, A.: Climatic variability during the last 90 ka of the southern and northern Levantine Basin as evident from marine records and speleothems, Quaternary Science Reviews, 28, 2882–2896, 2009.

Bar-Matthews, M., Ayalon, A., Kaufman, A., and Wasserburg, G. J.: The Eastern Mediterranean paleoclimate as a reflection of regional events: Soreq cave, Israel, Earth and Planetary Science Letters, 166, 85–95, 1999.

Bar-Matthews, M., Ayalon, A., and Kaufman, A.: Timing and hydrological conditions of sapropel events in the Eastern Mediterranean, as evident from speleothems, Soreq cave, Israel, Chemical Geology, 169, 145–156, 2000.

Bartov, Y., Goldstein, S. L., Stein, M., and Enzel, Y.: Catastrophic arid episodes in the Eastern Mediterranean linked with the North Atlantic Heinrich events, Geology, 31(5), 439–442, 2003.

Biscaye, P. E.: Distinction between kaolinite and chlorite in recent sediments by X-ray diffraction, The American Mineralogist, 49, 1281–1289, 1964.

Biscaye, P. E.: Mineralogy and sedimentation of recent deep-sea clay in the Atlantic Ocean and adjacent seas and oceans, Geological Society of America Bulletin, 76, 803–832, 1965.

Blanchet, C. L., Frank, M., and Schouten, S.: Asynchronous changes in vegetation, runoff and erosion in the Nile River watershed during the Holocene, PLoS One, 9(12), e115958, doi:10.1371/journal.pone.0115958, 2015.

Bolle, M.-P., Tantawy, A. A., Pardo, A., Adatte, T., Burns, S., and Kassab, A.: Climatic and environmental changes documented in the upper Paleocene and lower Eocene of Egypt, Eclogae Geologicae Helvetiae, 93, 33–51, 2000.

Bond, G., Broecker, W., Johnsen, S., McManus, J., Labeyrie, L., Jouzel, J., and Bonani, G.: Correlation between climate records from North Atlantic sediments and Greenland ice, Nature, 365, 143–147, 1993.

Bout-Roumazeilles, V., Combourieu Nebout, N., Peyron, O., Cortijo, E., Landais, A., and Masson-Delmotte, V.: Connection betweeen South Mediterranean climate and North African atmospheric circulation during the last 50,000 yr BP North

Atlantic cold events, Quaternary Science Reviews, 26, 3197–3215, 2007.
Box, M. R., Krom, M. D., Cliff, R. A., Bar-Matthews, M., Almogi-Labin, A., Ayalon, A., and Paterne, M.: Response of the Nile and its catchment to millenial-scale climatic change since the LGM from Sr isotopes and major elements of Eastern Mediterranean sediments, Quaternary Science Reviews, 30, 431–442, 2011.
Cacho, I., Grimalt, J. O., Pelejero, C., Canals, M., Sierro, F. J., Flores, J. A., and Shackleton, N.: Dansgaard-Oeschger and Heinrich event imprints in Alboran Sea paleotemperatures, Paleoceanography, 14, 698–705, 1999.
Cacho, I., Grimalt, J.O., Sierro, F. J., Shackleton, N., and Canals, M.: Evidence for enhanced Mediterranean thermohaline circulation during rapid climatic coolings, Earth and Planetary Science Letters, 183, 417–429, 2000.
Caley, T., Malaizé, B., Revel, M., Ducassou, E., Wainer, K., Ibrahim, M., Shoeaib, D., Migeon, S., and Marieu, V.: Orbital timing of the Indian, East Asian and African boreal monsoons and the concept of a "global monsoon", Quaternary Science Reviews, 30, 3705–3715, 2011.
Chester, R., Baxter, G. G., Behairy, A. K. A., Connor, K., Cross, D., Elderfield, H., and Padgham, R. C.: Soil-sized eolian dusts from the lower troposphere of the eastern Mediterranean Sea, Marine Geology, 24, 201–217, 1977.
Claussen, M., Bathiany, S., Brovkin, V., and Kleinen, T.: Simulated climate-vegetation interaction in semi-arid regions affected by plant diversity, Nature Geoscience, 6, 954–958, 2013.
deMenocal, P., Ortiz, J., Guilderson, T., Adkins, J., Sarnthein, M., Baker, L., and Yarusinsky, M.: Abrupt onset and termination of the African Humid Period: rapid climate responses to gradual insolation forcing, Quaternary Science Reviews, 19, 347–361, 2000.
Ducassou, E., Migeon, S., Capotondi, L., and Mascle, J.: Run-out distance and erosion of debris-flows in the Nile deep-sea fan system: Evidence from lithofacies and micropalaeontological analyses, Marine and Petroleum Geology, 39, 102–123, 2013.
Ehrmann, W., Schmiedl, G., Hamann, Y., Kuhnt, T., Hemleben, C., and Siebel, W.: Clay minerals in late glacial and Holocene sediments of the northern and southern Aegean Sea, Palaeogeography, Palaeoclimatology, Palaeoecology, 249, 36–57, 2007.
Ehrmann, W., Seidel, M., and Schmiedl, G.: Dynamics of Late Quaternary North

African humid periods documented in the clay mineral record of central Aegean Sea sediments, Global and Planetary Change, 107, 186–195, 2013.

Emeis, K.-C., Sakamoto, T., Wehausen, R., and Brumsack, H.-J.: The sapropel record of the eastern Mediterranean Sea - results of Ocean Drilling Program Leg 160, Palaeogeography, Palaeoclimatology, Palaeoecology, 158, 371–395, 2000.

Emeis, K.-C., Schulz, H., Struck, U., Rossignol-Strick, M., Erlenkeuser, H., Howell, M. W., Kroon, D., Mackensen, A., Ishizuka, S., Oba, T., Sakamoto, T., and Koizumi, I.: Eastern Mediterranean surface water temperatures and $\delta^{18}O$ composition during deposition of sapropels in the late Quaternary, Paleoceanography, 18, 1005, doi:10.1029/2000PA000617, 2003.

Fontugne, M. R. and Calvert, S. E.: Late Pleistocene variability of the carbon isotopic composition of organic matter in the Eastern Mediterranean: Monitor of changes in carbon sources and atmospheric CO_2 concentrations, Paleoceanography, 7, 1–20, 1992.

Foucault, A. and Stanley, D. J.: Late Quaternary paleoclimatic oscillations in East Africa recorded by heavy minerals in the Nile delta, Nature, 3390, 44–46, 1989.

Foucault, A. and Mélières, F.: Palaeoclimatic cyclicity in central Mediterranean Pliocene sediments: the mineralogical signal, Palaeogeography, Palaeoclimatology, Palaeoecology, 158, 311–323, 2000.

Garzanti, E., Ando, S., Padoan, M., Vezzoli, G., and El Kammar, A.: The modern Nile sediment system: Processes and products, Quaternary Science Reviews, 130, 9–56, 2015.

Gasse, F.: Hydrological changes in the African tropics since the Last Glacial Maximum, Quaternary Science Reviews, 19, 189–211, 2000.

Gasse, F., Chalie, F., Vincens, A., Williams, M. A. J., and Williamson, D.: Climatic patterns in equatorial and southern Africa from 30,000 to 10,000 years ago reconstructed from terrestrial and near-shore proxy data, Quaternary Science Reviews, 27, 2316–2340, 2008.

Grant, K. M., Rohling, E. J., Bar-Matthews, M., Ayalon, A., Medina-Elizalde, M., Bronk Ramsey, C., Satow, C., and Roberts, A. P.: Rapid coupling between ice volume and polar temperature over the past 150,000 years, Nature, 491, 744–747, 2012.

Grelaud, M., Marino, G., Ziveri, P., Rohling, E. J.: Abrupt shoaling of the nutricline in

response to massive freshwater flooding at the onset of the last interglacial sapropel event, Paleoceanography 27, PA3208, doi:3210.1029/2012PA002288, 2012.
Hamann, Y., Ehrmann, W., Schmiedl, G., Krüger, S., Stuut, J.-B., and Kuhnt, T.: Sedimentation processes in the Eastern Mediterranean Sea during the Late Glacial and Holocene revealed by end-member modelling of the terrigenous fraction in marine sediments, Marine Geology, 248, 97–114, 2008.
Hamann, Y., Ehrmann, W., Schmiedl, G., and Kuhnt, T.: Modern and late Quaternary clay mineral distribution in the area of the SE Mediterranean Sea, Quaternary Research, 71, 453–464, 2009.
Hemleben, C., Hoernle, K., Jørgensen, B.B., and Roether, W. (Eds.): Ostatlantik – Mittelmeer – Schwarzes Meer, Cruise No. 51, 12 September – 28 December 2001, Meteor-Berichte, Universität Hamburg, 03-01, 225 pp., 2003.
Holeman, J. N.: The sediment yield of major rivers of the world, Water Resources Research, 4, 737–747, 1968.
Kallel, N., Duplessy, J.-C., Labeyrie, L., Fontugne, M., Paterne, M., and Montacer, M.: Mediterranean pluvial periods and sapropel formation over the last 200 000 years, Palaeogeography, Palaeoclimatology, Palaeoecology, 157, 45–58, 2000.
Koho, K. A., García, R., de Stigter, H. C., Epping, E., Koning, E., Kouwenhoven, T. J., and Van der Zwaan, G. J.: Sedimentary labile organic carbon and pore water redox control on species distribution of benthic foraminifera: A case study from Lisbon-Setúbal Canyon (southern Portugal), Progress in Oceanography, 79, 55–82, 2008.
Krom, M. D., Michard, A., Cliff, R. A., and Strohle, K.: Sources of sediment to the Ionian Sea and western Levantine basin of the Eastern Mediterranean during S-1 sapropel times, Marine Geology, 160, 45–61, 1999a.
Krom, M. D., Cliff, R. A., Eijsink, L. M., Herut, B., and Chester, R.: The characterisation of Saharan dusts and Nile particulate matter in surface sediments from the Levantine basin using Sr isotopes, Marine Geology, 155, 319–330, 1999b.
Krom, M. D., Stanley, J. D., Cliff, R. A., and Woodward, J. C.: Nile River sediment fluctuations over the past 7000 yr an their key role in sapropel development, Geology, 30, 71–74, 2002.
Kröpelin, S., Verschuren, D., Lézine, A.-M., Eggermont, H., Cocquyt, C., Francus, P.,

Cazet, J.-P., Fagot, M., Rumes, B., Russell, J. M., Darius, F., Conley, D. J., Schuster, M., von Suchodoletz, H., and Engstrom, D. R.: Climate-driven ecosystem succession in the Sahara: The past 6000 years, Science, 320, 765–768, 2008.

Lamb, H. F., Bates, C. R., Coombes, P. V., Marshall, M. H., Umer, M., Davies, S. J., and Dejen, E.: Late Pleistocene desiccation of Lake Tana, source of the Blue Nile, Quaternary Science Reviews, 26, 287–299, 2007.

Lisiecki, L. E. and Raymo, M. E.: A Pliocene-Pleistocene stack of 57 globally distributed benthic $\delta^{18}O$ records, Paleoceanography, 20, (PA1003), doi:10.1029/2004PA001071, 2005.

Lourens, L. J., Antonarakou, A., Hilgen, F. J., Van Hoof, A. A. M., Vergnaud-Grazzini, C., and Zachariasse, W. J.: Evaluation of the Plio-Pleistocene astronomical timescale, Paleoceanography, 11, 391–413, 1996.

Löwemark, L., Lin, Y., Chen, H.-F., Yang, T.-N., Beier, C., Werner, F., Lee, C.-Y., Song, S.-R., and Kao, S.-J.: Sapropel burn-down and ichnological response to late Quaternary sapropel formation in two ~400 ky records from the eastern Mediterranean Sea, Palaeogeography, Palaeoclimatology, Palaeoecology, 239, 406–425, 2006.

Maldonado, A. and Stanley, D. J.: Clay mineral distribution patterns as influenced by depositional processes in the southeastern Levantine Sea, Sedimentology, 28, 21–32, 1981.

Manning, K. and Timpson, A.: The demographic response to Holocene climate change in the Sahara, Quaternary Science Reviews, 101, 28–35, 2014.

Marino, G., Rohling, E.J., Rodriguez-Sanz, L., Grant, K. M., Heslop, D., Roberts, A. P., Stanford, J. D., and Yu, J.: Bipolar seesaw control on last interglacial sea level, Nature, 522, 197–201, 2015.

Marshall, M. H., Lamb, H. F., Huws, D., Davies, S. J., Bates, R., Bloemendal, J., Boyle, J., Leng, M. J., Umer, M., and Bryant, C.: Late Pleistocene and Holocene drought events at Lake Tana, the source of the Blue Nile, Global and Planetary Change, 78, 147–161, 2011.

Martrat, B., Jimenez-Amat, P., Zahn, R., and Grimalt, J. O.: Similarities and dissimilarities between the last two deglaciations and interglaciations in the North Atlantic region, Quaternary Science Reviews, 99, 122–134, 2014.

Milliman, J. D. and Syvitski, J. P. M.: Geomorphic/tectonic control of sediment discharge to the ocean: the importance of small mountainous rivers, Journal of

Geology, 100, 525–544, 1992.

Moreno, A., Cacho, I., Canals, M., Prins, M. A., Sanchez-Goni, M.-F., Grimalt, J. O., and Weltje, G. J.: Saharan dust transport and high-latitude glacial climatic variability: the Alboran Sea record, Quaternary Research, 58, 318–328, 2002.

Morigi, C.: Benthic environmental changes in the Eastern Mediterranean Sea during sapropel S5 deposition, Palaeogeography, Palaeoclimatology, Palaeoecology, 273, 258–271, 2009.

Mothersill, J. S.: The mineralogy and geochemistry of the sediments of northwestern Lake Victoria, Sedimentology, 23, 553–565, 1976.

Müller, U. C., Pross, J., Tzedakis, P. C., Gamble, C., Kotthoff, U., Schmiedl, G., Wulf, S., and Christanis, K.: The role of climate in the spread of modern humans into Europe, Quaternary Science Reviews, 30, 273–279, 2011.

Mulitza, S., Prange, M., Stuut, J.-B., Zabel, M., von Dobeneck, T., Itambi, A. C., Nizou, J., Schulz, M., and Wefer, G.: Sahel megadroughts triggered by glacial slowdowns of Atlantic meridional overturning, Paleoceanography, 23, PA4206, doi:10.1029/2008PA001637, 2008.

Nyakairu, G. W. A. and Koeberl, C.: Mineralogical and chemical composition and distribution of rare earth elements in clay-rich sediments from central Uganda, Geochemical Journal, 35, 13–28, 2001.

Osborne, A. H., Vance, D., Rohling, E. J., Barton, N., Rogerson, M., and Fello, N.: A humid corridor across the Sahara for the migration of early modern humans out of Africa 120,000 years ago, PNAS, 105, 16444–16447, 2008.

Osborne, A. H., Marino, G., Vance, D., and Rohling, E. J.: Eastern Mediterranean surface water Nd during Eemian sapropel S5: monitoring northerly (mid-latitude) versus southerly (sub-tropical) freshwater contributions, Quaternary Science Reviews, 29, 2473–2483, 2010.

Pachur, H.-J. and Hoelzmann, P.: Late Quaternary palaeoecology and palaeoclimates of the eastern Sahara, Journal of African Earth Sciences, 30, 929–939, 2000.

Paillard, D., Labeyrie, L., and Yiou, P.: Macintosh program performs time-series analysis, Eos Transactions, American Geophysical Union, 77, 379, 1996.

Petschick, R.: MacDiff 4.2.5. http://www.geologie.uni-frankfurt.de/staff/homepages/petschick/petschick.html (last access 15 December 2015) 2001.

Pickard, G. L. and Emery, W. J.: Descriptive Physical Oceanography, Pergamon

Press, 320 pp., 1990.

Pross, J., Koutsodendris, A., Christanis, K., Fischer, T., Fletcher, W. J., Hardiman, M., Kalaitzidis, S., Knipping, M., Kotthoff, U., Milner, A. M., Müller, U. C., Schmiedl, G., Siavalas, G., Tzedakis, P. C., and Wulf, S.: The 1.35-Ma-long terrestrial climate archive of Tenaghi Philippon, northeastern Greece: Evolution, exploration, and perspectives for future research, Newsletter on Stratigraphy, 48/3, 253–276, 2015.

Quelennec, R. E. and Kruc, C. B.: Nile suspended load and its importance for the Nile delta morphology. UNDP/UNESCO Proceedings of the Seminar on Nile Delta Sedimentation. Alexandria, Academy of Scientific Research and Technology, Egypt, 1–257, 1976.

Reimer, P. J., Bard, E., Bayliss, A., Beck, J. W., Blackwell, P. G., Bronk Ramsey, C., Buck, C. E., Cheng, H., Edwards, R. L., Friedrich, M., Grootes, P. M., Guilderson, T. P., Haflidason, H., Hajdas, I., Hatté, C., Heaton, T. J., Hoffmann, D. L., Hogg, A. G., Hughen, K. A., Kaiser, K. F., Kromer, B., Manning, S. W., Niu, M., Reimer, R. W., Richards, D. A., Scott, E. M., Southon, J. R., Staff, R. A., Turney, C. S. M., and van der Plicht, J.: IntCal13 and Marine13 radiocarbon age calibration curves 0–50,000 years cal BP. Radiocarbon, 55, 1869–1887, 2013.

Renssen, H., Brovkin, V., Fichefet, T., and Goosse, H.: Simulation of the Holocene climate evolution in Northern Africa: The termination of the African Humid Period, Quaternary International, 150, 95–102, 2006.

Revel, M., Ducassou, E., Grousset, F. E., Bernasconi, S. M., Migeon, S., Revillon, S., Mascle, J., Murat, A., Zaragosi, S., and Bosch, D.: 100,000 Years of African monsoon variability recorded in sediments of the Nile margin, Quaternary Science Reviews, 29, 1342–1362, 2010.

Rohling, E.: Review and new aspects concerning the formation of eastern Mediterranean sapropels, Marine Geology, 122, 1–28, 1994.

Rohling, E. J., Gieskes, W. W. C.: Late Quaternary changes in Mediterranean intermediate water density and formation rate, Paleoceanography, 4, 531–545, 1989.

Rohling, E. J., Mayewski, P. A., Abu-Zied, R. H., Casford, J. S. L., and Hayes, A.: African monsoon variability during the previous interglacial maximum, Earth and Planetary Science Letters, 202, 61–75, 2002a.

Rohling, E. J., Mayewski, P. A., Abu-Zied, R. H., Casford, J. S. L., and Hayes, A.:

Holocene atmosphere-ocean interactions: records from Greenland and the Aegean Sea, Climate Dynamics, 18, 587–593, 2002b.

Rohling, E. J., Marino, G., and Grant, K. M.: Mediterranean climate and oceanography, and the periodic development of anoxic events (sapropels), Earth-Science Reviews, 143, 62–97, 2015.

Rossignol-Strick, M.: African monsoons, an immediate climate response to orbital insolation, Nature, 304, 46–49, 1983.

Rossignol-Strick, M., Nesteroff, W., Olive, P., and Vergnaud-Grazzini, C.: After the deluge: Mediterranean stagnation and sapropel formation, Nature, 295, 105–110, 1982.

Sandler, A. and Herut, B.: Composition of clays along the continental shelf off Israel: contribution of the Nile versus local sources, Marine Geology, 167, 339–354, 2000.

Scheuvens, D., Schütz, L., Kandler, K., Ebert, M., and Weinbruch, S.: Bulk composition of northern African dust and its source sediments - A compilation, Earth-Science Reviews, 116, 170–194, 2013.

Schmiedl, G., Mitschele, A., Beck, S., Emeis, K.-C., Hemleben, C., Schulz, H., Sperling, M., and Weldeab, S.: Benthic foraminiferal record of ecosystem variability in the eastern Mediterranean Sea during times of sapropel S5 and S6 deposition, Palaeogeography, Palaeoclimatology, Palaeoecology, 190, 139–164, 2003.

Schmiedl, G., Kuhnt, T., Ehrmann, W., Emeis, K.-C., Hamann, Y., Kotthoff, U., Dulski, P., and Pross, J.: Climatic forcing of eastern Mediterranean deep-water formation and benthic ecosystems during the past 22000 years, Quaternary Science Reviews, 29, 3006–3020, 2010.

Shanahan, T. M., McKay, N. P., Hughen, K. A., Overpeck, J. T., Otto-Bliesner, B., Heil, C. W., King, J., Scholz, C. A., and Peck, J.: The time-transgressive termination of the African Humid Period, Nature Geoscience, 8, 140–144, 2015.

Stager, J. C., Ryves, D. B., Chase, B. M., and Pausata, F. S. R.: Catastrophic drought in the Afro-Asian monsoon region during Heinrich Event 1, Science, 331, 1299–1302, 2011.

Stanley, D. S. and Wingerath, J. G.: Clay mineral distributions to interpret Nile Cell provenance and dispersal: I. Lower River Nile to delta sector, Journal of Coastal Research, 12, 911–929, 1996a.

Stanley, D. J. and Wingerath, J. G.: Nile sediment dispersal altered by the Aswan High Dam: The kaolinite trace, Marine Geology, 133, 1–9, 1996b.

Stanley, D. J., Mart, Y., and Nir, Y.: Clay mineral distributions to interpret Nile Cell provenance and dispersal: II. Coastal plain from Nile Delta to northern Israel, Journal of Coastal Research, 13, 506–533, 1997.

Stanley, D. J., Nir, Y., and Galili, E.: Clay mineral distributions to interpret Nile Cell provenance and dispersal: III. Offshore margin between Nile delta and northern Israel, Journal of Coastal Research, 14, 196–217, 1998.

Tjallingii, R., Claussen, M., Stuut, J.-B. W., Fohlmeister, J., Jahn, A., Bickert, T., Lamy, F., and Röhl, U.: Coherent high- and low-latitude control of the northwest African hydrological balance, Nature Geoscience, 1, 670–675, 2008.

Tzedakis, P. C.: Vegetation variability in Greece during the last interglacial, Geologie en Mijnbouw, 79, 355–367, 2000.

Venkatarathnam, K. and Ryan, W. B. F.: Dispersal patterns of clay minerals in the sediments of the eastern Mediterranean Sea, Marine Geology, 11, 261–282, 1971.

Weaver, C. E. and Beck, K. C.: Miocene of the S.E. United States: A model for chemical sedimentation in a peri-marine environment, Sedimentary Geology, 17, 1–234, 1977

Wehausen, R. and Brumsack, H.-J.: The formation of Pliocene Mediterranean sapropels: constraints from high-resolution major and minor element studies, in: Proceedings of the Ocean Drilling Program, Scientific Results, edited by: Robertson, A. H. F., Emeis, K.-C., Richter, C., and Camerlenghi, A., 160, Ocean Drilling Program, College Station, TX, 207–217, 1998.

Wehausen, R. and Brumsack, H. J.: Chemical cycles in Pliocene sapropel-bearing and sapropel-barren eastern Mediterranean sediments, Palaeogeography, Palaeoclimatology, Palaeoecology, 158, 325–352, 2000.

Weldeab, S., Emeis, K.-C., Hemleben, C., and Siebel, W.: Provenance of lithogenic surface sediments and pathways of riverine suspended mattern in the Eastern Mediterranean Sea: evidence from $^{143}Nd/^{144}Nd$ and $^{87}Sr/^{86}Sr$ ratios, Chemical Geology, 186, 139-149, 2002.

Weldeab, S., Emeis, K.-C., Hemleben, C., Schmiedl, G., and Schulz, H.: Spatial productivity variations during formation of sapropels S5 and S6 in the Mediterranean Sea: evidence from Ba contents, Palaeogeography,

Palaeoclimatology, Palaeoecology, 191, 169–190, 2003.

Weldeab, S., Menke, V., and Schmiedl, G.: The pace of East African monsoon evolution during the Holocene, Geophysical Research Letters, 41, doi:10.1002/2014GL059361, 2014.

Williams, M., Talbot, M., Aharon, P., Salaam, Y. A., Williams, F., and Brendeland, K. I.: Abrupt return of the summer monsoon 15,000 years ago: new supporting evidence from the lower White Nile valley and Lake Albert, Quaternary Science Reviews, 25, 2651–2665, 2006.

Williams, M. A. J.: Late Pleistocene and Holocene environments in the Nile basin, Global and Planetary Change, 69, 1–15, 2009.

Williams, M. A. J., Usai, D., Salvatori, S., Williams, F. M., Zerboni, A., Maritan, L., and Linseele, V.: Late Quaternary environments and prehistoric occupation in the lower White Nile valley, central Sudan, Quaternary Science Reviews, 130, 72–88, 2015.

TABLE CAPTIONS

Table 1. Metadata for the investigated sediment core GeoTü SL110 and other cores mentioned in the text (cf. Fig. 1).

Table 2. Data used for constructing the age model for the investigated sediment core GeoTü SL110. Oxygen isotope ages are based on a graphical correlation with the LC21 record (Grant et al., 2012) from the southern Aegean Sea. ~~Oxygen isotope ages follow Lisiecki and Raymo (2005). The age of the base of S5 is according to Bar-Matthews et al. (2000), Rohling et al. (2002), Morigi (2009) and Osborne et al. (2010~~).

FIGURE CAPTIONS

Figure 1. Location map of the Nile River basin and the Eastern Mediterranean Sea. **(a)** The Nile River and its main tributaries. Blue dashed lines indicate wadis. The green dotted line shows the main outcrop of Cenozoic basalts in Ethiopia. Also shown are the northern summer and winter limits of the African rain belt (red dashed lines, ARB-S, ARB-W, after Blanchet et al., 2014). Black arrows in the Eastern Mediterranean Sea indicate the surface currents (after Pickard and Emery, 1990). **(b)** Map of the southeastern Levantine Sea with the location of the investigated sediment core GeoTü SL110 and other cores mentioned in the text; not shown are GeoTü SL143 and LC21, which are positioned further to the north (cf. Table 1). D.B. = Damietta branch of the Nile in the delta, R.B. = Rosetta branch.

Figure 2. Depth-Age plot for the investigated sediment core GeoTü SL110 (red). The age points are listed in Table 2. For comparison, corresponding data were extracted ~~calculated~~ for core MD84-641 (blue, Fontugne and Calvert, 1992: Table 1). Marine Isotope Stages (MIS) follow Lisiecki and Raymo (2005).

Figure 3. Basic data of core GeoTü SL110. **(a)** $\delta^{18}O$ of *G. ruber*, lightness (*L**), % total organic carbon (TOC), ~~and~~ % sand and silt/clay ratio of the terrigenous sediment fraction, and linear sedimentation rates (LSR, cm/ka). **(b)** clay mineral percentages of smectite, illite, kaolinite, chlorite and palygorskite. Gray bars mark the position of sapropel layers S1, S3, S4, S5 and the pre-sapropelic layer beneath S5 (light grey). Marine Isotope Stages (MIS) are indicated. ~~The top of S5 corresponds to a hiatus.~~

Figure 4. Combination of the June insolation at 65°N **(a)**, the Saharan dust record in the central Aegean Sea core GeoTü SL143 (**b**; Ehrmann et al., 2013), the Nile discharge based on Fe data in the Nile delta (**c**; Revel et al., 2010, age model by Caley et al., 2011), and the Nile sediment discharge based on Ka_r **(d)** and Sm_r **(e)** at site GeoTü SL110. Grey bars indicate the positions of sapropels S1, S3, S4, S5 and of the pre-sapropelic layer (light grey) beneath S5 in core in SL110. Heinrich Events (H) are flagged with arrows. Marine Isotope Stages (MIS) and African Humid Periods (AHP) are indicated at the bottom.

Table 1. Metadata for the investigated sediment core GeoTü SL110 and other cores mentioned in the text (cf. Fig. 1).

Core	Latitude (°N)	Longitude (°E)	Water depth depth (m)	Reference
GeoTü SL110	32°38.95’	34°06.22’	1437	this study
GeoTü KL83	32°36.87’	34°08.89’	1431	Weldeab et al. (2002)
GeoTü SL112	32°44.52’	34°39.02’	892	Hamann et al. (2008, 2009)
GeoTü SL143	38°15.71’	25°06.19’	665	Ehrmann et al. (2013)
MD84-641	33°02’	32°38’	1375	Fontugne and Calvert (1992)
9501	34°32’	33°59’	980	Almogi-Labin et al. (2009)
9509	32°01’	34°16’	884	Almogi-Labin et al. (2009)
MS27PT	31°47.90’	29°27.70’	1389	Revel et al. (2010)
LC21	35°40´	26°35´	1522	Grant et al. (2012)

Table 2. Data used for constructing the age model for the investigated sediment core GeoTü SL110. Oxygen isotope ages are based on a graphical correlation with the LC21 record (Grant et al., 2012) from the southern Aegean Sea. ~~Oxygen isotope ages follow Lisiecki and Raymo (2005). The age of the base of S5 is according to Bar-Matthews et al. (2000), Rohling et al. (2002), Morigi (2009) and Osborne et al. (2010).~~

Depth cm	Age cal. ka BP	Data
0.00	0.00	Sediment surface
34.50	6.43	^{14}C AMS dating
64.50	11.53	^{14}C AMS dating
150.50	24.38	^{14}C AMS dating
189.11	29.29	LC21
234.50	33.92	^{14}C AMS dating
254.50	36.29	LC21
359.54	53.50	LC21
465.30	67.11	LC21
509.55	84.99	LC21
529.23	89.03	LC21
554.51	103.32	LC21
569.46	107.79	LC21
579.50	110.38	LC21
598.00	119.00	Hiatus end
598.00	126.00	Hiatus start
603.00	128.00	LC21
624.52	131.94	LC21

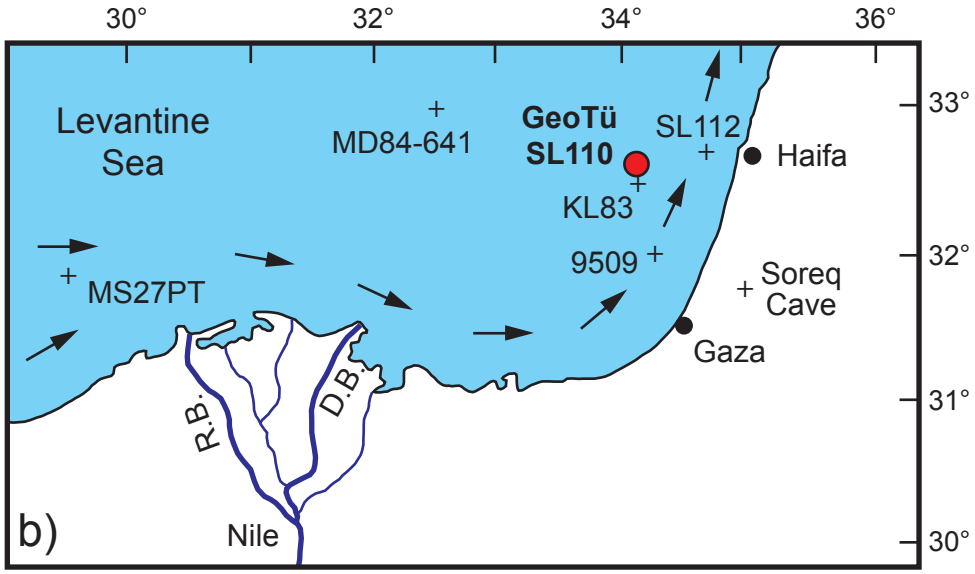

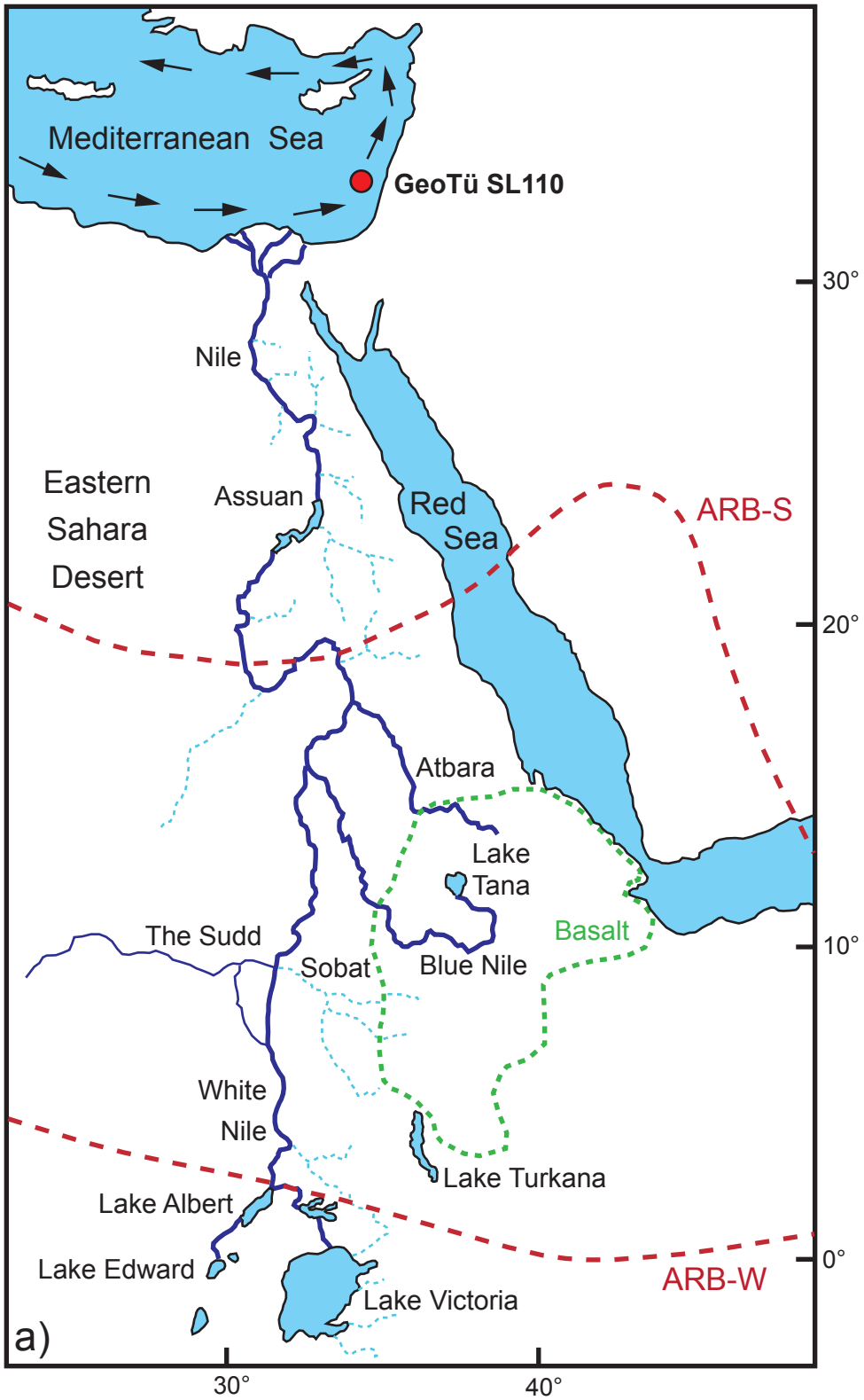

Figure 1
Ehrmann et al.

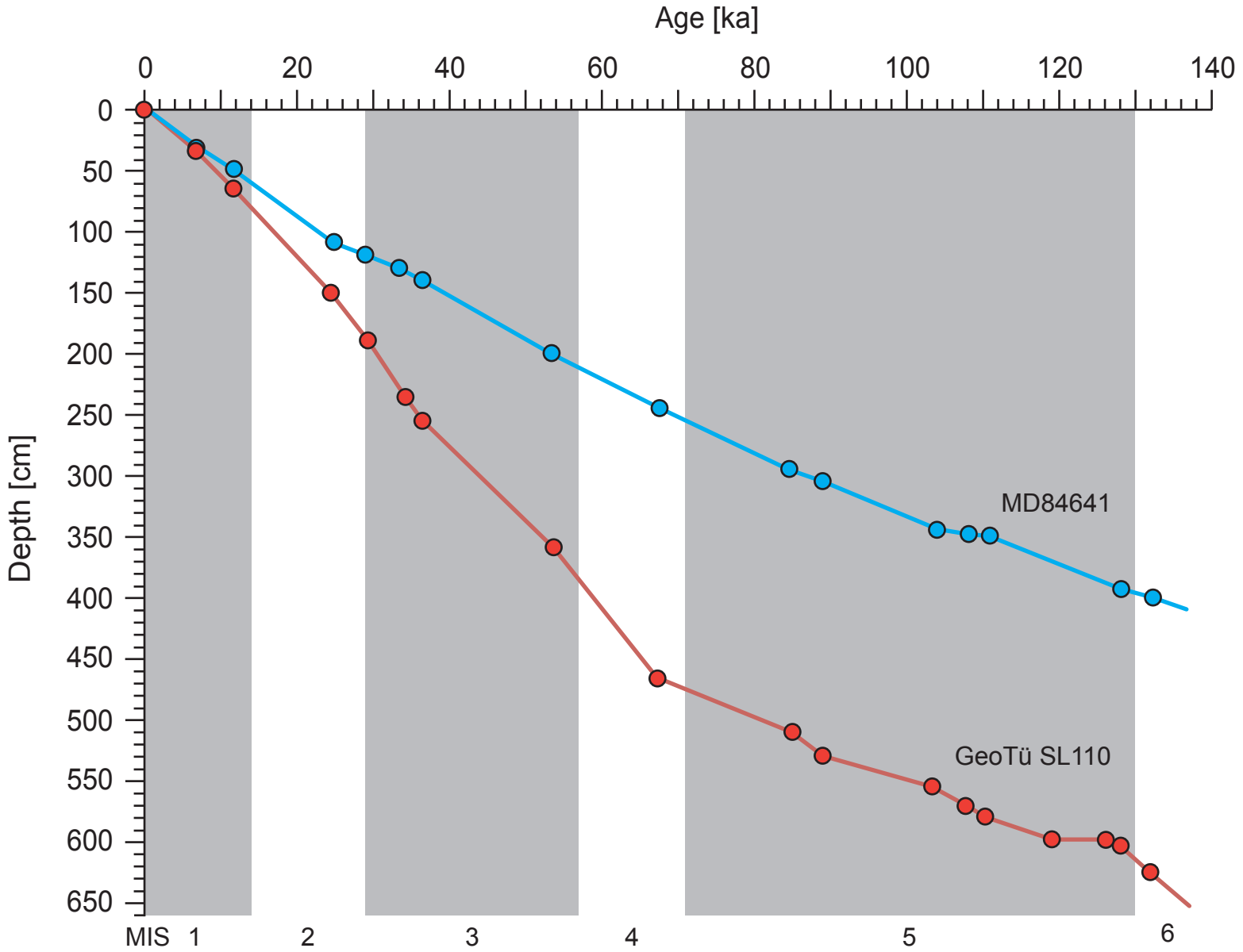

Figure 2 - Ehrmann et al.

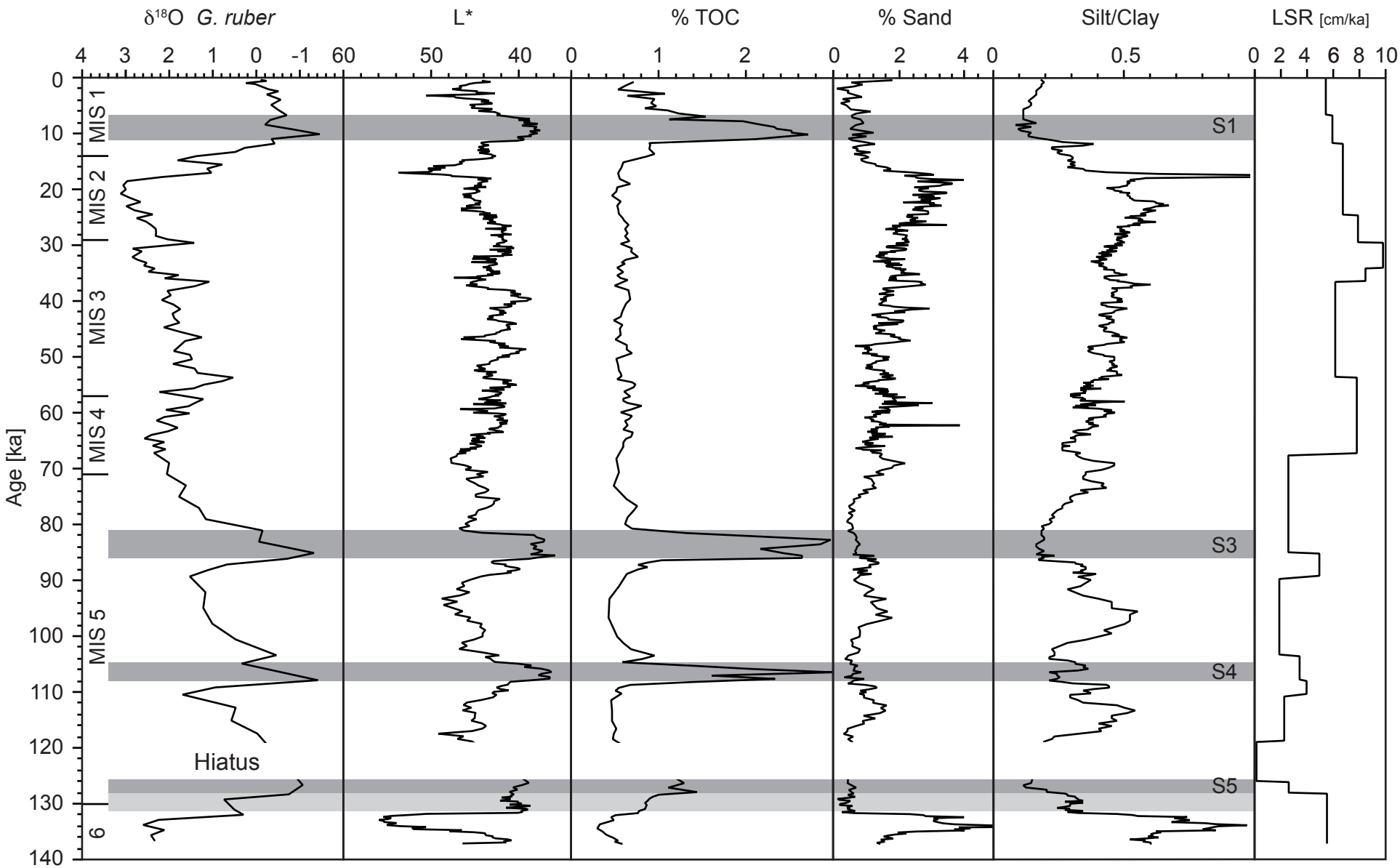

Figure 3a - Ehrmann et al.

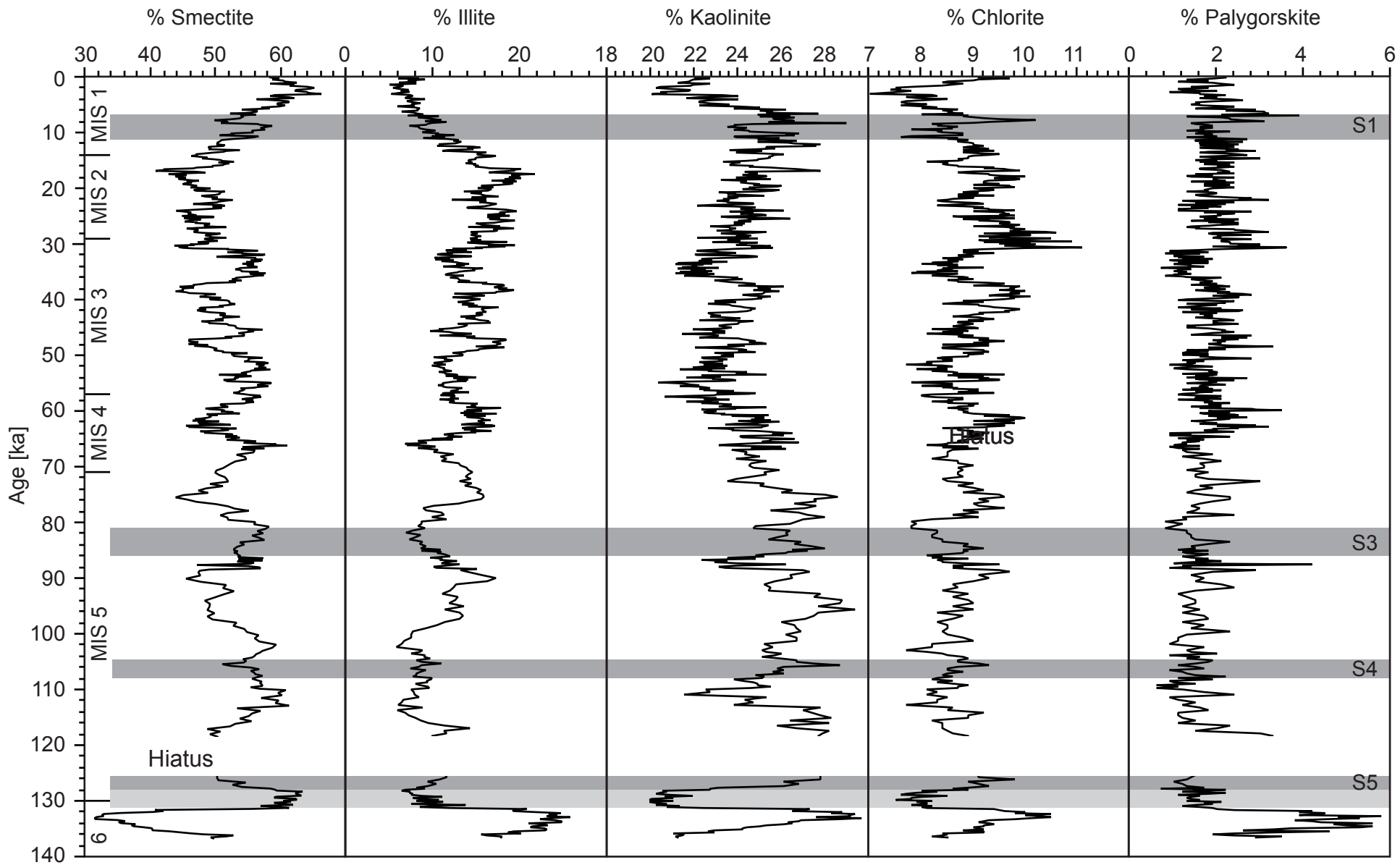

Figure 3b - Ehrmann et al.

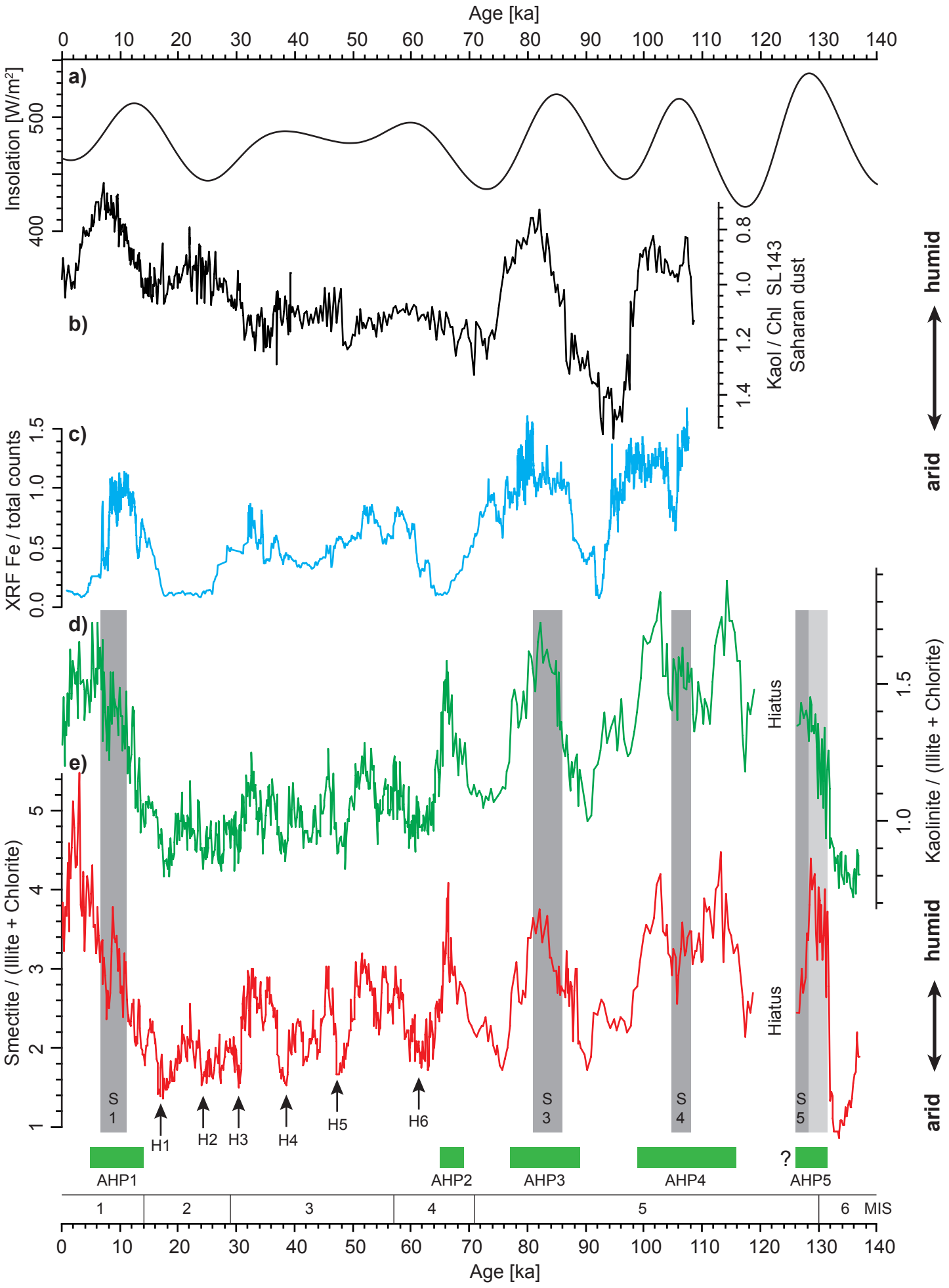

Figure 4 - Ehrmann et al.